Journal of Solid State Chemistry 182 (2009) 1666–1672

Contents lists available at ScienceDirect

Journal of Solid State Chemistry

journal homepage: www.elsevier.com/locate/jssc

Structural investigation of $K_xBa_{1-x}Ga_{2-x}Ge_{2+x}O_8$ solid solutions using the X-ray Rietveld method

Ni Qin [a,*], Marjeta Maček Kržmanc [a], Anton Meden [b], Danilo Suvorov [a]

[a] Advanced Materials Department, Jožef Stefan Institute, Jamova 39, 1000 Ljubljana, Slovenia
[b] Faculty of Chemistry and Chemical Technology, University of Ljubljana, Aškerčeva 5, 1000 Ljubljana, Slovenia

ARTICLE INFO

Article history:
Received 6 October 2008
Received in revised form
4 March 2009
Accepted 10 March 2009
Available online 20 March 2009

Keywords:
LTCC
Synthetic feldspar
Rietveld structure refinement
Phase transition

ABSTRACT

The $K_xBa_{1-x}Ga_{2-x}Ge_{2+x}O_8$ ($x = 0.6-1.0$) solid solutions undergo a structural phase transition that has a significant effect on their sintering behavior and their microwave dielectric properties. The crystal structures of both phases within the solid-solution region were determined by the Rietveld method using powder X-ray diffraction data. We found that the low-temperature-stable phase is isostructural with the pseudo-orthorhombic $KGaGe_3O_8$ (space group $P2_1/a$), while the high-temperature-stable phase has a typical monoclinic feldspar structure (space group $C2/m$). Due to the topological differences between the two structures, the T–O bonds within the tetrahedra must be partially recombined to make a new framework, which causes an endothermic effect during the $P2_1/a$ to $C2/m$ phase transition. The correlation between the crystal structures, the microwave dielectric properties and the phase-transition behaviors were discussed in terms of the crystallographic features, the lattice parameters, and the strain-induced anisotropic peak-broadening.

1. Introduction

Feldspar is an important mineral that makes up a large proportion of the Earth's crust and is a traditional ingredient in the manufacture of glass. However, recently a novel application of feldspar in low-temperature cofired-ceramic (LTCC) technology, based on its low softening temperature and low manufacturing costs, was reported [1,2]. It was found that the cofiring temperature of commercial LTCC pastes can be lowered to 800–850 °C by introducing a large amount of glass into the dielectric oxides. Unfortunately, however, the advantage of the glass additive is offset by deleterious influences, such as high dielectric losses and a low mechanical strength. In our research group we are currently investigating a material based on the gallogermanate-feldspar. Compared with commercially available materials for LTCC tapes, which are mainly based on aluminosilicate and borosilicate feldspars, the gallogermanate feldspars exhibit rapid crystallization along with more attractive properties, including a low sintering temperature (~900 °C), a low permittivity ($\varepsilon_r = 5-7$), small temperature coefficients ($\tau_f \sim -20$ ppm/°C) and, most importantly, a high quality factor (the maximum $Q \times f$ exceeds 100,000 GHz at ~13 GHz) [3,4].

In our previous work [3,4] on the $K_xBa_{1-x}Ga_{2-x}Ge_{2+x}O_8$ solid solutions, a reversible phase transition was observed at 840–990 °C depending on the composition ($0.6 \leqslant x \leqslant 1$) and the direction of the phase transition (Table 1). The low-temperature-stable phase (subsequently referred to as the "low phase") that was synthesized and sintered at temperatures below the phase-transition point exhibited a much higher $Q \times f$, a smaller ε_r and a similar τ_f compared with the high-temperature-stable phase (subsequently referred to as the "high phase"). A crystallographic investigation of both phases should provide us with useful information about the correlation between the crystal structure and the microwave dielectric properties, as well as the abnormal aging effect of $KGaGe_3O_8$ (corresponding to $x = 1$), as described in Ref. [4].

Moreover, crystallographic information about $K_xBa_{1-x}Ga_{2-x}Ge_{2+x}O_8$ is also of great interest to the mineral-science community. The $K_xBa_{1-x}Ga_{2-x}Ge_{2+x}O_8$ solid solutions lie on the tie-line between $KGaGe_3O_8$ and $BaGa_2Ge_2O_8$. Neither of the end-members can be formed naturally because of the rarity of Ga in the Earth's crust. So far, most of the investigations on feldspars have concentrated on natural minerals. In contrast, little is known about synthetic feldspars.

It was for these reasons that we decided to analyze the crystal structures of $K_xBa_{1-x}Ga_{2-x}Ge_{2+x}O_8$ ($0.6 \leqslant x \leqslant 1$) solid solutions, with respect to the phase transition and LTCC applications, by a powder X-ray diffraction (XRD) method based on a Rietveld refinement. The correlation between the crystal structures, the microwave dielectric properties and the phase-transition behaviors were discussed in terms of the crystallographic features, the lattice parameters, and the strain-induced anisotropic peak-broadening (APB).

2. Experimental section

Stoichiometric mixtures of reagent-grade powders of K_2CO_3 (Alfa Aesar 99.997%, dried at 200 °C), $BaCO_3$ (Alfa Aesar 99.8%),

* Corresponding author. Fax: +386 1 477 3875.
E-mail address: qinniijs@gmail.com (N. Qin).

0022-4596/$ - see front matter © 2009 Elsevier Inc. All rights reserved.
doi:10.1016/j.jssc.2009.03.004

Table 1
The lowest temperature for the $P2_1/a \Rightarrow C2/m$ transition to occur ($T_{P\to C}$), the annealing temperature for the $C2/m \Rightarrow P2_1/a$ transition to yield the fastest kinetics ($T_{C\to P}$) and the melting point (T_m) of the $K_xBa_{1-x}Ga_{2-x}Ge_{2+x}O_8$ solid solutions ($0.6 \leqslant x \leqslant 1$).

Composition x	$T_{P\to C}$ (°C)	$T_{C\to P}$ (°C)	T_m (°C)
1	900	840	1005
0.9	920	860	1056
0.67	980	900	1158
0.6	990	940	1170

Ga_2O_3 (Alfa Aesar 99.99%) and GeO_2 (Alfa Aesar 99.999%) were fired at 950–1020 °C to yield a high-phase regime. The low-phase powders were obtained by prolonged annealing of the high phase at 840–860 °C for up to 100 h. (Details of the kinetic study on the phase transition were reported previously in a related study [4].) The powders were ground with acetone in an agate mortar and filtered with a 15 μm mesh screen before drying at 200 °C.

The XRD data for the Rietveld refinement were collected at room temperature in reflection θ–2θ geometry on an X'pert PRO MPD diffractometer (PANalytical B.V., Almelo, the Netherlands) with an incident beam monochromator for pure Cu$K\alpha$1 radiation. Primary and secondary Soller slits of 0.02 rad, vertical mask of 10 mm and variable divergence and antiscatter slits were used, so that a constant area of 10×10 mm of sample was irradiated throughout the measurement. Full measuring range of a 128-channel linear multi-strip X'Celerator detector was applied to scan the range from 5° to 140° 2θ in steps of 0.017° with an effective time per step of 2000 s. Total collection time was about 34 h.

3. Results and discussion

3.1. Rietveld structure refinement

From the XRD patterns, the low phase of all the investigated compositions appeared to be isostructural with the monoclinic $KGaGe_3O_8$, of which the β is nearly 90° and the symmetry is very close to orthorhombic. The structure refinement was thus initiated using the reported space group ($P2_1/a$) and the atomic coordinates for $KGaGe_3O_8$ (ICSD No. 1022) [5] with the substitutional Ba atoms incorporated into the K atomic sites. The high phase was refined on the basis of the monoclinic lattice of the disordered $KFeGe_3O_8$ feldspar (space group $C2/m$, ICSD No. 59390) [5] by substituting Ga for Fe.

The XRD data were analyzed by the Rietveld method using the fundamental-parameters (FPs) approach contained within the software TOPAS V2.1 (Bruker-AXS) [6]. The experimental parameters, the crystallographic data and the refinement details are listed in Table 2.

The background was described by a 12-order polynomial function. All the refinable atomic coordinates were varied independently along with the unit-cell parameters. Full occupancies in all the atomic sites were assumed and the fractional occupancy of the K atoms in the M-sites, denoted as O_K, was refined. The fractional occupancies of the Ba, Ga and Ge atoms were constrained by the equations $O_{Ba} = 1-O_K$, $O_{Ga} = (2-O_K)/4$ and $O_{Ge} = (2+O_K)/4$ with respect to the local charge balance. In particular, the O_K with composition $x = 1$ was set to 1. Since the Ga and Ge atoms have similar scattering factors, it does not make a big difference if their occupancies are refined independently. Scattering factors were used for the neutral atoms. The isotropic atomic displacement parameters of the same elements in different sites were constrained equally.

A trial correction for the preferred orientation (PO) using either a March Dollase item [7] in up to two directions or a 4-order spherical harmonics (SH) series [8] was examined. The former correction led to a small decrease in the R values (for instance, R_{wp} decreased from 4.85% to 4.61% for the $P2_1/a$ structure with $x = 0.67$). Meanwhile, the parameter that represents the degree of PO deviated from 1 (corresponding to an ideal sample without any PO) in a very small range (0.98–1.02) in all the characteristic crystalline directions. The SH correction for the PO resulted in smaller R values ($R_{wp} = 4.37\%$ for the same sample) and was therefore employed in the final refinement.

As for the refinement of the $C2/m$ structure, much higher R_{wp} values (10–14%) were initially obtained with the same approach. The mismatch between the measured and refined profiles was subjected to an APB phenomenon, as shown in Fig. 1, in which the full width at half-maximum (FWHM) of the individual peaks of the $C2/m$ structure fluctuated on a larger scale compared with the $P2_1/a$ structure. In order to simulate the contribution of the APB to the XRD profile, an 8-order SH correction was introduced to the Lorentzian half width in the launch mode, as provided by the TOPAS program (see Ref. [6], p. 94 for the functions). The resulting R_{wp} were 7.28% and 9.15% for $x = 0.9$ and $x = 1$, respectively.

The refinement with the smallest R values for each composition was selected for the discussion. As shown in Fig. 2, the

Table 2
Lattice parameters and selected details of the structural refinement of the $K_xBa_{1-x}Ga_{2-x}Ge_{2+x}O_8$ solid solutions.

X	1	0.9	0.67	0.6	1	0.9
Space group	$P2_1/a$	$P2_1/a$	$P2_1/a$	$P2_1/a$	$C2/m$	$C2/m$
a (Å)	9.4902	9.4684	9.4277	9.4172	8.8675	8.8613
b (Å)	9.8943	9.8936	9.8927	9.8904	13.6401	13.6318
c (Å)	8.7228	8.7319	8.7496	8.7536	7.4928	7.4921
β (°)	89.998	89.996	89.996	89.998	115.916	115.741
V (Å^3)	819.06	817.97	816.04	815.30	815.14	815.20
Z	4	4	4	4	4	4
PO[a]	Yes	Yes	Yes	Yes	No	No
APB[b]	No	No	No	No	Yes	Yes
R_{exp}	1.18	1.28	1.21	1.22	1.18	1.24
R_{wp}	6.78	5.03	4.37	4.72	9.15	7.28
R_p	4.86	3.78	3.25	3.48	6.54	5.27

The square root of the residual variants are smaller than 1 at the last decimal place and are therefore unpresented in the manuscript.
[a] PO: SH correction for preferred orientation.
[b] APB: SH correction for anisotropic peak-broadening.

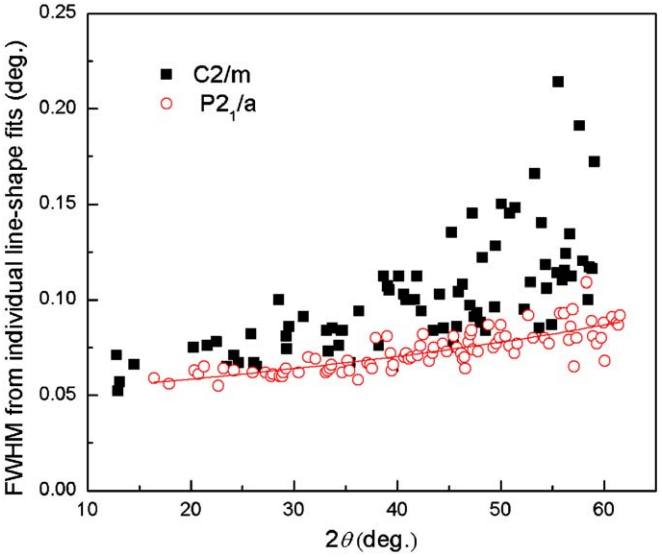

Fig. 1. FWHM versus diffraction angle 2θ for $KGaGe_3O_8$. The widths of the pseudo-Voigt fits to individual peaks are plotted.

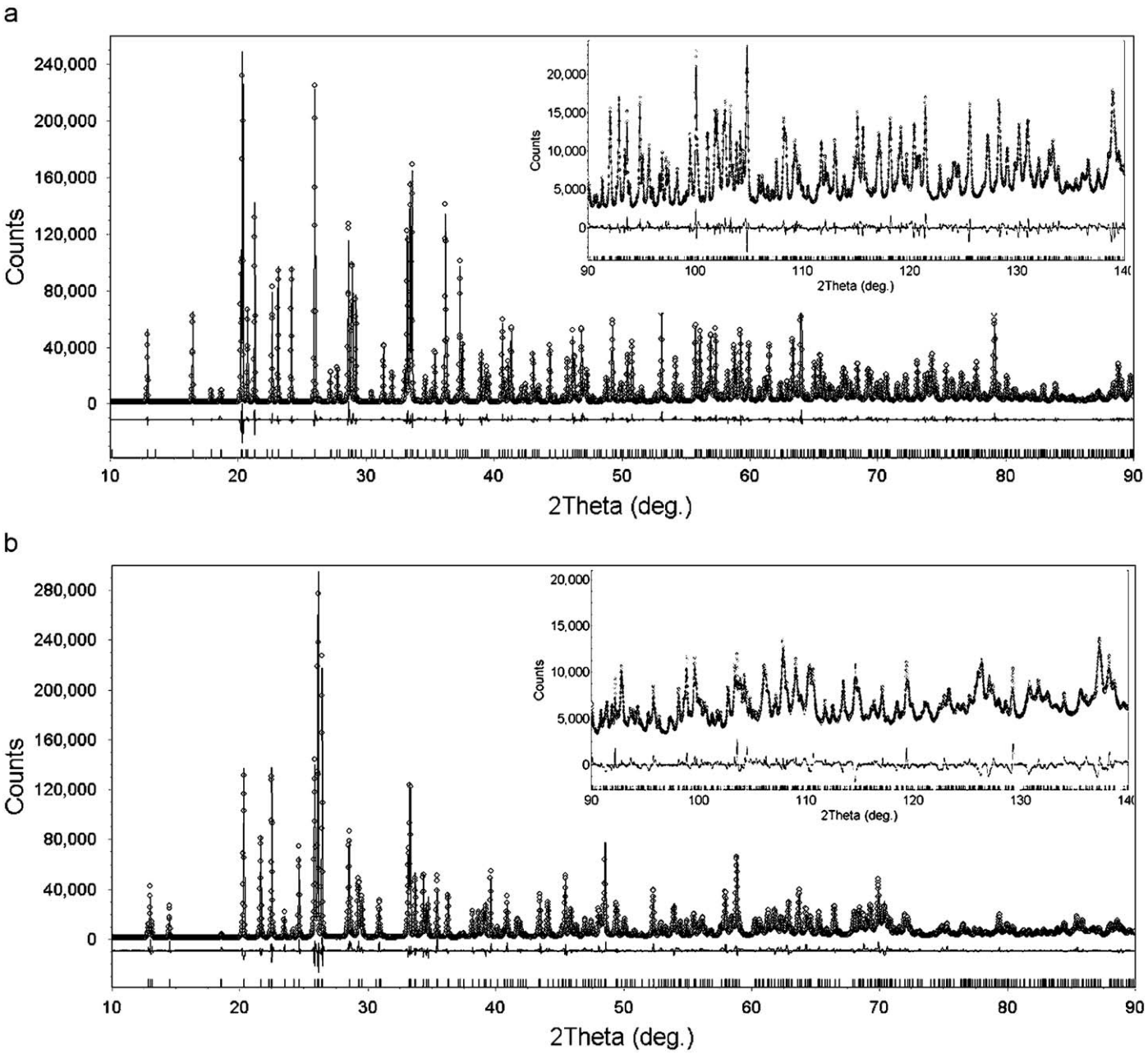

Fig. 2. Final Rietveld plots of (a) the low-temperature-stable phase (space group $P2_1/a$) and (b) the high-temperature-stable phase (space group $C2/m$) of $KGaGe_3O_8$ (corresponding to $x = 1$ in $K_xBa_{1-x}Ga_{2-x}Ge_{2+x}O_8$). Circles represent measured intensity, and the solid curve, the calculated intensity. The difference curve is plotted below. Vertical bars at the bottom indicate the positions of the Bragg reflections.

calculated XRD profile agrees well with the experimental data across the whole range of examined angles. The high-angle diffraction peaks exhibited a sharp and clear profile for all the $P2_1/a$-crystallized samples as well as the $C2/m$ phase of the $K_xBa_{1-x}Ga_{2-x}Ge_{2+x}O_8$ ($x = 1$ and 0.9), indicating a sufficiently high crystallization in these samples. As for the $C2/m$ samples with $x = 0.67$ and 0.6, the XRD measurements exhibited peaks that were too broad at high angles. Therefore, the refinement of these two samples will not be discussed here.

3.2. Topological differences between the two structures

The refined structures of the low and high phases of the $K_xBa_{1-x}Ga_{2-x}Ge_{2+x}O_8$ solid solution are shown in Figs. 3 and 4, respectively. Except for minor shifts in the atomic positions and the occupancies of the individual atoms, the investigated solid solutions with different compositions are isostructural with the model compounds.

As the main feature of the feldspar structure, the frameworks of both phases are composed of GeO_4/GaO_4 tetrahedra, which connect to each other by sharing the corners and forming 4- and 8-member rings. The interstices within the 8-member rings are occupied by K or Ba atoms. In spite of the difference in lattice symmetry, the topological analogy between the two structures with respect to the tetrahedral configuration is evident from comparing the (001) projections of the $P2_1/a$ structure (Fig. 3(b)) and the $(20\bar{1})$ projection of the $C2/m$ structure (Fig. 4(b)). An algebraic code developed by Smith and Rinaldi [9] can be used to describe the topological relations between the two structures, in

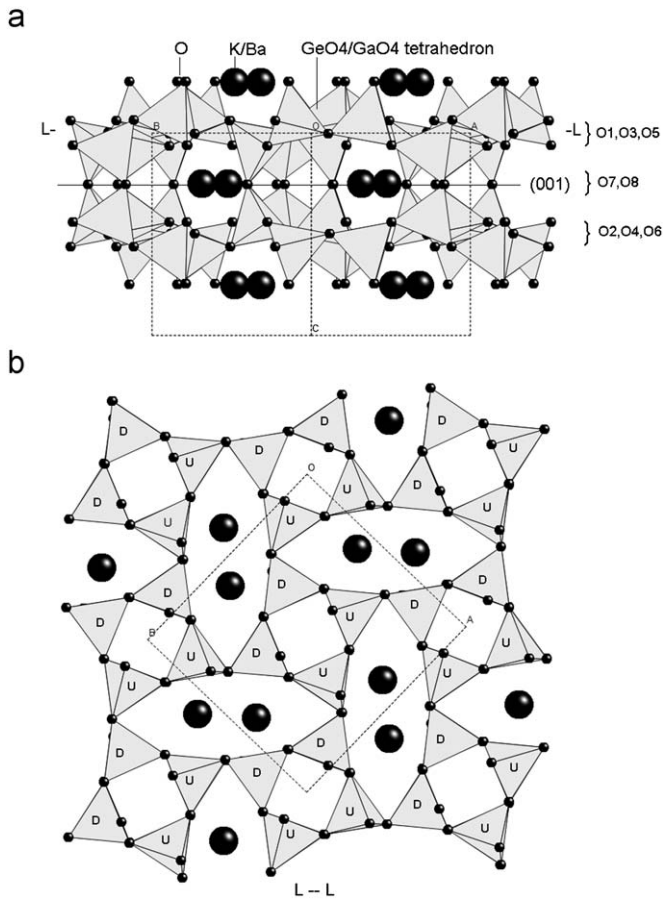

Fig. 3. (a) The *b*-axis projection of the $K_xBa_{1-x}Ga_{2-x}Ge_{2+x}O_8$ ($P2_1/a$) structure and (b) the projection of a tetrahedral sheet on a (001) plane, where a tetrahedron pointing up is denoted as U and one pointing down is denoted as D.

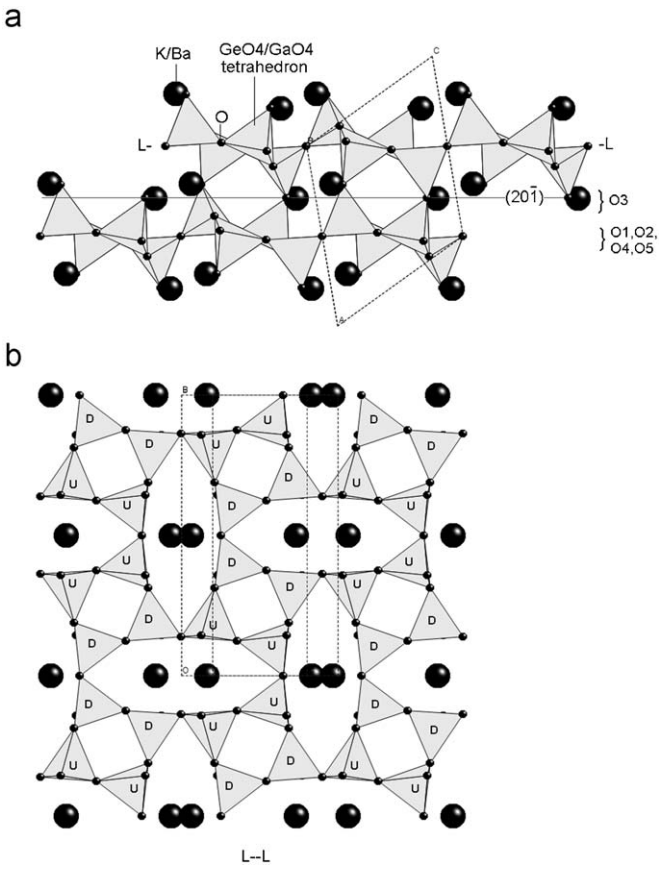

Fig. 4. (a) The *b*-axis projection of the $K_xBa_{1-x}Ga_{2-x}Ge_{2+x}O_8$ ($C2/m$) structure and (b) the projection of a tetrahedral sheet on a (20$\bar{1}$) plane.

which a tetrahedron pointing up is denoted as U and one pointing down is denoted as D. The 4-member ring of both structures exhibited a rigid UUDD configuration (Fig. 3(b)). The 8-member rings in the $P2_1/a$ structure have a characteristic UDUUDUDD configuration, while the $C2/m$ structure has two different types: the UUUUDDDD and the DUUDUDDU (Fig. 4(b)).

A comparison between the two structures clearly indicates their differences at a fundamental level. For this reason, the conversion between the two structures cannot be simply achieved by distorting the framework of the lattice without changing the connection between the adjacent tetrahedra. Functionally, the *T*–O bonds must be partially destroyed before being re-associated to construct a new framework. Such a reaction is usually accompanied by a thermal effect. An intensive endothermic peak was already observed during a differential thermal analysis in the $P2_1/a$ to $C2/m$ phase transition in $K_xBa_{1-x}Ga_{2-x}Ge_{2+x}O_8$ ($x = 0.6-1$) [4].

3.3. Lattice parameters, bond lengths, bond angles and coordination of M atoms

The lattice parameters of both structures as functions of the composition x are plotted in Fig. 5. The unit-cell volume of the samples with the $P2_1/a$ structure increases nearly linearly with increasing x, in proportion to the mean ionic radius [10] of the K^+ (1.46 Å, 7-coordination) and the Ba^{2+} (1.38 Å, 7-coordination) admixture. Instead of expanding in all directions, the lattice elongates only in the *a*-axis, shrinks in the *c*-axis and remains almost constant in the *b*-axis. The relative differences in the *a*-, *b*- and *c*-axial lengths between the end members of the investigated compositions ($KGaGe_3O_8$ and $K_{0.6}Ba_{0.4}Ga_{1.4}Ge_{2.6}O_8$) are 0.8%, 0.04% and −0.4%, respectively. It turns out that the variation in the lattice parameter along the *a*-axis dominated the change in the unit-cell volume. The angle β is very close to 90° and almost constant across the range of compositions.

Fig. 6 shows the variation of the mean T_i-O ($i = 1, 2, 3$ and 4) bond length of the $P2_1/a$ structure with the value of x. Since the data points for the $C2/m$ structure are too few to show a trend, only the results of the $P2_1/a$ structure are discussed here. The divergent tendency of the *T*–O distances with decreasing x is clearly seen in Fig. 6, where the *T*1-O and *T*2-O bonds tend to shrink, while the *T*3-O and *T*4-O bonds tend to lengthen. Smith and Brown [11] discussed, in a general review on feldspar minerals that an individual *T*–O bond length depends in particular on the type of *T*-atoms. Since the ionic radius of the Ga^{3+} (0.47 Å, 4-coordination) is larger than that of the Ge^{4+} (0.39 Å, 4-coordination), a longer *T*–O distance can be expected if the *T* site is preferentially occupied by Ga. The increase of the *T*3-O and *T*4-O bond lengths with the increasing Ga content (corresponding to a decreasing x) might be a reflection of the preferential occupation of Ga in the *T*3 and *T*4 sites. An example of this trend was shown in the well-known paracelsian ($BaAl_2Si_2O_8$, corresponding to $x = 0$ when written as $K_xBa_{1-x}Al_{2-x}Si_{2+x}O_8$), for which the Al/Si atomic ratio is 1, and the *T*3/*T*4 and *T*1/*T*2 sites are separately occupied by Al and Si atoms [12].

The individual O–*T*–O angles of the $P2_1/a$ structure of the $K_xBa_{1-x}Ga_{2-x}Ge_{2+x}O_8$ ($x = 0.6-1.0$) solid solutions vary in the

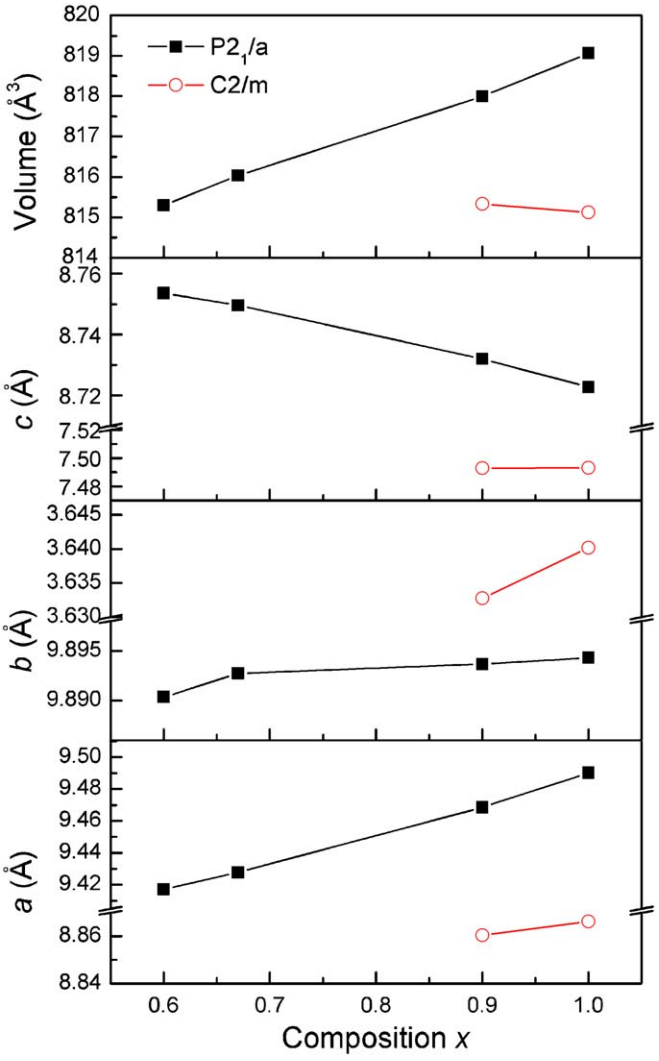

Fig. 5. Unit-cell parameters of the $K_xBa_{1-x}Ga_{2-x}Ge_{2+x}O_8$ solid solutions as functions of composition. The error bars are smaller than the symbols.

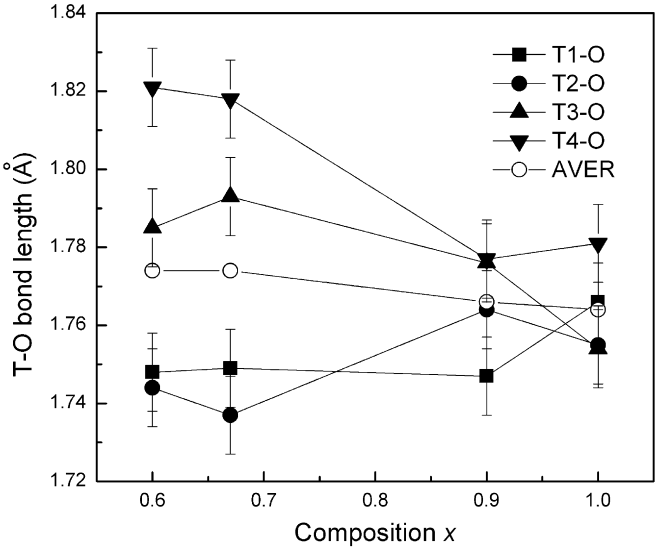

Fig. 6. *T*–O distances in $P2_1/a$ $K_xBa_{1-x}Ga_{2-x}Ge_{2+x}O_8$ ($x = 0.6$–1) solid solutions.

range 100°–121°, embraced in the surveyed range (96°–123°) for all reported feldspars [11]. Any deviation from the theoretical O–*T*–O angle (109°28′) indicates a distortion from the ideal. In the present case, the smallest distortion of the intra-tetrahedral angles is observed in the *T*3-related tetrahedra for all the investigated compositions, while the angles associated with *T*1, *T*2 and *T*4 have a broader distribution range in the samples with a lower K concentration compared with $KGaGe_3O_8$ (Fig. 7).

The total range of the inter-tetrahedral *T*–O–*T* angles is 120°–136° in the $P2_1/a$ structure and 126°–145° in the *C*2/*m* structure. In the $P2_1/a$ structure (Fig. 3 (a)), O1, O2, O3, O4 and O5 atoms are located at the joints of the tetrahedral sheets within the (001) plane, and they have smaller inter-tetrahedral angles than those (O6, O7 and O8) located at the joints between the layers. Similar results were also observed in the isomeric *C*2/*m* structure (Fig. 4(a)), in which the O3 atom at the joints between the layers has the largest *T*–O–*T* angle, while those within the parallel tetrahedral sheets (O1, O2, O4 and O5) have smaller *T*–O–*T* angles. The variation of the individual *T*–O–*T* angle with the change in composition is not consistent enough for us to comment on.

A 7-fold and 9-fold coordination of oxygen to the *M* atoms (K and/or Ba) were automatically established by the program TOPAS V2.1 for the $P2_1/a$ and the *C*2/*m* structures, respectively. The individual *M*–O bond distances vary in the range 2.7–3.1 Å, and the average *M*–O bond distance in the $P2_1/a$ structure is 7% shorter than that in the *C*2/*m* structure. In principle, the dielectric constant measured at microwave frequencies is basically determined by the electronic and ionic polarizabilities, and the contribution of the heavy cations is usually the most important effect. Since the *M*-O distance in the *C*2/*m* structure is longer than that in the $P2_1/a$ structure, there is more space for the heavy *M*-cations to vibrate in the *C*2/*m* structure under the periodic force of an electric field, which in turn results in a higher permittivity. The theoretical dielectric constant of $K_xBa_{1-x}Ga_{2-x}Ge_{2+x}O_8$ ceramics was calculated with the Clausius–Mosotti equation using the ionic polarizability values (α_D) determined by Shannon [13], and compared with the experimental data in Table 3. Although the calculated ε_r is smaller than the experimental value, the variation in the trend of the calculated ε_r versus the composition agrees well with the experimental result.

3.4. APB in the C2/m samples

As we mentioned before, an APB was observed in the *C*2/*m* structure and a pronounced improvement in the pattern-fit was achieved by using a SH correction for the peak widths. The APB is generally associated with intragranular factors such as lattice strains, defects and limitations in the spatial extent of the coherently scattering domains (especially the grain shape). In the present work, however, no obvious elongation of the grains was observed in the $K_xBa_{1-x}Ga_{2-x}Ge_{2+x}O_8$ ceramics with a scanning electron microscope. A further investigation would be needed to clarify the nature of this peak-broadening phenomenon in the *C*2/*m* structure.

On the other hand, an abnormal aging effect was observed in the *C*2/*m*-type $KGaGe_3O_8$ when investigating the kinetics of the *C*2/*m* to $P2_1/a$ phase transition [4]. By "aging effect" we mean that the transition rate decreases rapidly with the aging time under the same experimental conditions. The XRD measurement showed no difference in the phase constitution of the aged *C*2/*m* powders. A possible reason for the aging phenomenon may be that the $P2_1/a$ structure of the $KGaGe_3O_8$ (corresponding to $x = 1$) has a much larger unit-cell volume than the *C*2/*m* structure (Fig. 5), and the variation of the lattice volume may have an important

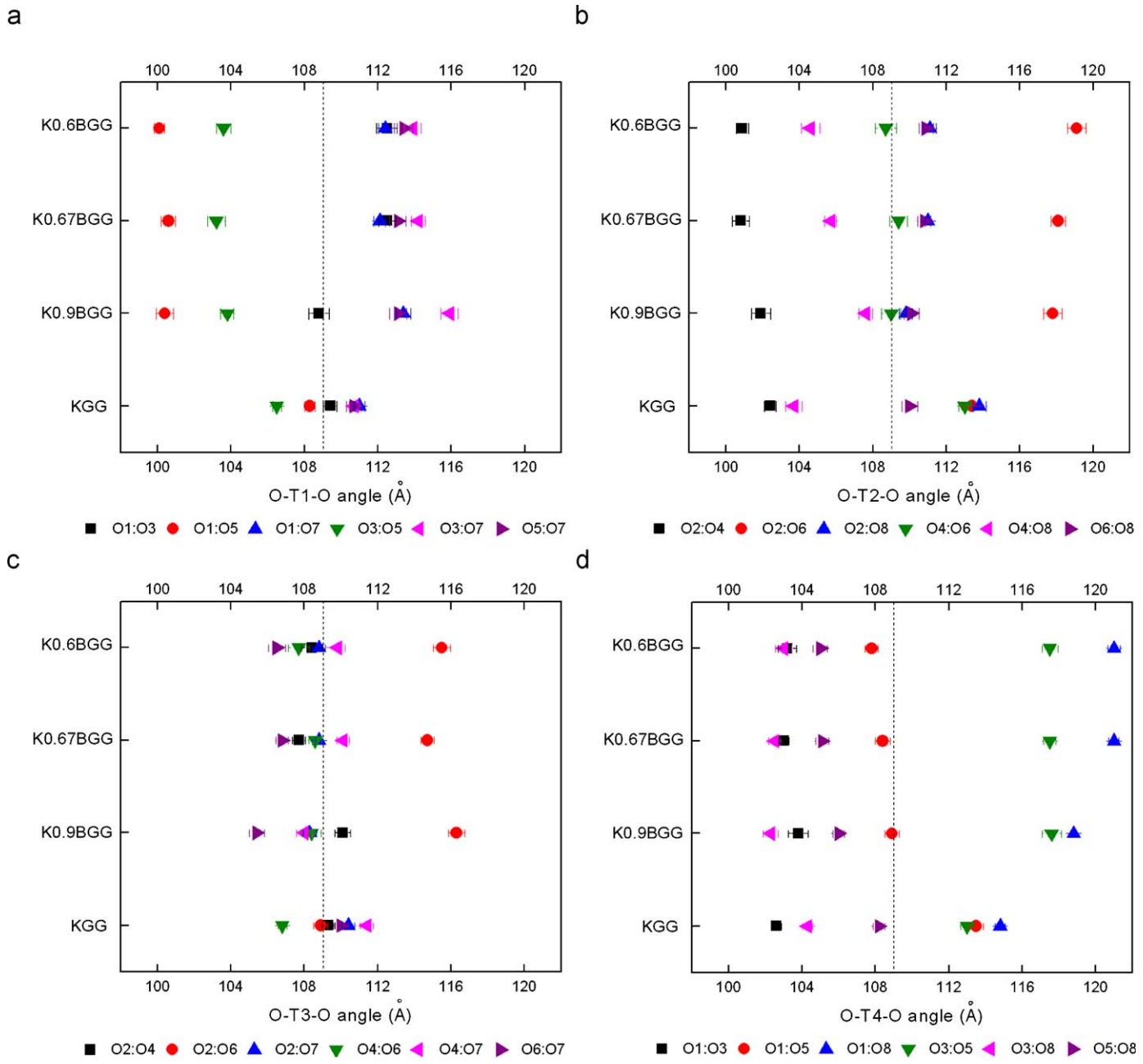

Fig. 7. Intra-tetrahedral angles O–*T*–O associated with (a) *T*1, (b) *T*2, (c) *T*3 and (d) *T*4 in the $P2_1/a$ $K_xBa_{1-x}Ga_{2-x}Ge_{2+x}O_8$ ($x = 0.6$–1) solid solutions.

Table 3
Comparison of the calculated and the measured dielectric constants (at ~13 GHz) of the $K_xBa_{1-x}Ga_{2-x}Ge_{2+x}O_8$ solid solutions.

Composition x	Space group	α_D (Å^3)	V_m (Å^3)	ε_{calc}	ε_{exp}
1	$P2_1/a$	26.3	204.77	4.49	5.5
	$C2/m$	26.3	203.78	4.53	6.2
0.9	$P2_1/a$	26.54	204.49	4.58	5.6
	$C2/m$	26.54	203.80	4.60	6.6
0.67	$P2_1/a$	27.11	204.01	4.76	6.0
0.6	$P2_1/a$	26.30	203.83	4.83	6.1

influence on the kinetics of the phase transition. With respect to the energy transitions that eventually occur in a structural phase transition, any kinds of strains that adapt to the expansionary tendency of the framework will make the phase transition easier. The $KGaGe_3O_8$ is especially sensitive to strain because of the large change in unit-cell volume via the phase transition. Since such a situation existed when the $C2/m$ powders were cooled from the synthesizing temperature, an internal strain was thermally produced in the product. With part of the strain released gradually over time, the driving force of the phase transition degrades as well when the powders are reheated to the phase-transition temperature, which in turn leads to a decrease in the phase-transition rate.

The APB observed in the $C2/m$-type samples might be evidence of the existence of internal strains. In the process of the SH correction for the APB, the Lorentzian half width of each individual peak was corrected by multiplying the 8-order SH, which represents the scale of the lattice strain in the corresponding crystallographic direction. A large, positive SH

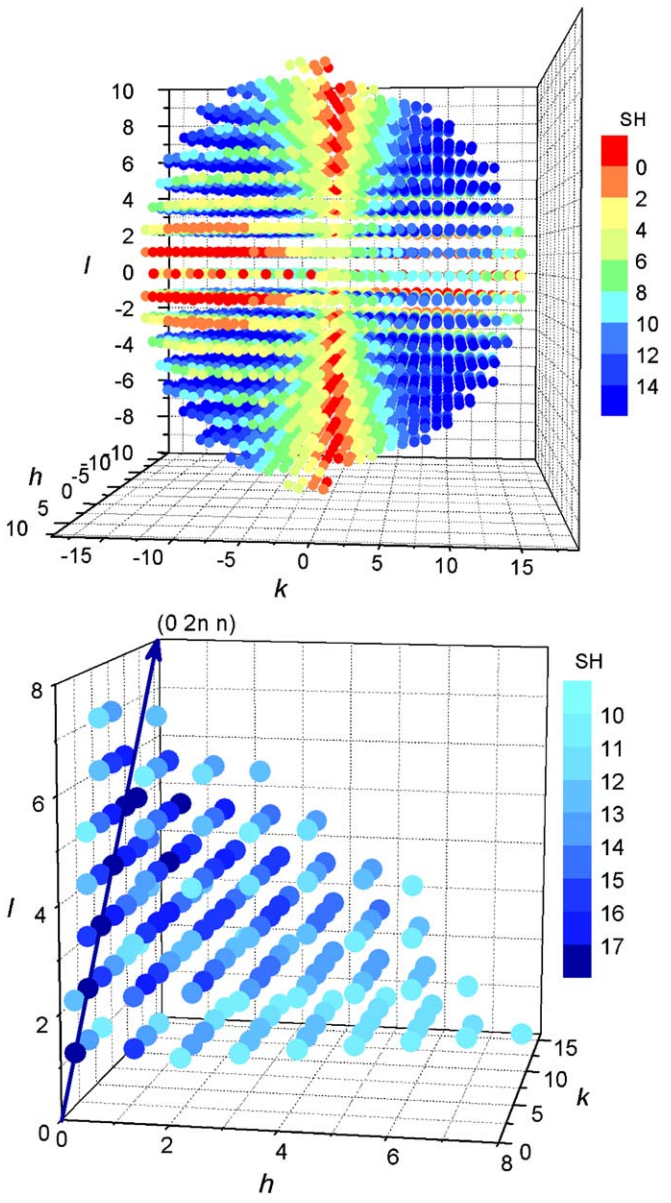

Fig. 8. The 3-D plots of the refined width scaling parameter (SH) of individual X-ray reflection peaks versus the Miller indices in a rectangular coordinate system.

corresponds to an extraordinarily broad diffraction peak. The refined SH factors are plotted versus the Miller indices in Fig. 8, taking into account that the $(\bar{h}\bar{k}l)$ and $(\bar{h}k\bar{l})$ diffractions have the same Bragg angle with (hkl). Note that the (hkl) plot is presented in a rectangular coordinate system but not in reciprocal space. The maximum SH was observed on the $(02nn)$ planes with $n = 1, 2$, etc. The centralized distribution of the SH plots around the $(02nn)$ vectors implies a PO of the strains along these directions.

4. Conclusion

The crystal structures of both the low-temperature-stable and high-temperature-stable phases of the $K_xBa_{1-x}Ga_{2-x}Ge_{2+x}O_8$ solid solutions were refined in the composition range $0.6 \leqslant x \leqslant 1$ using the X-ray Rietveld method. We found that the low-temperature-stable phase is isostructural with the pseudo-orthorhombic $KGaGe_3O_8$ (space group $P2_1/a$), while the high-temperature-stable phase has a typical monoclinic feldspar structure (space group $C2/m$). A topological interpretation of the differences between the two structures was given in terms of the linkage between the tetrahedral sheets. Due to the differences in the fundamental features of the topology, the T–O bonds in the crystal structure have to be partially disassociated and reconnected to form the new phase, which led to an intensive thermal effect during the phase transition.

The variation of the lattice parameter along the a-axis versus the composition x dominated the change in the unit-cell volume. The divergent tendency of the T–O distances with decreasing x was associated with a preferential occupation of Ga in the $T3$ and $T4$ sites. The $C2/m$ phase has a higher dielectric constant than the $P2_1/a$ phase due to the longer M–O bond distance. The variation in the dielectric constant with composition is dominated by the ionic polarizablity of the M cations. The anisotropic peak-broadening observed in the $C2/m$ samples implies the existence of internal strains in the lattice, which might be responsible for the low $Q \times f$ value of the $C2/m$ samples and the aging effect of the $C2/m$ to $P2_1/a$ phase transition in $KGaGe_3O_8$.

Acknowledgement

The work was supported by Slovene human resources development and scholarship fund.

Appendix A. Supplementary material

Supplementary data associated with this article can be found in the online version at doi:10.1016/j.jssc.2009.03.004.

References

[1] C.L. Lo, J.G. Duh, B.S. Chiou, J. Am. Ceram. Soc. 85 (2002) 2230–2235.
[2] V.M.F. Marques, D.U. Tulyaganov, S. Agathopoulos, V. Kh. Gataullin, G.P. Kothiyal, J.M.F. Ferreira, J. Eur. Ceram. Soc. 26 (2006) 2503–2510.
[3] M.M. Kržmanc, A. Meden, D. Suvorov, J. Eur. Ceram. Soc. 27 (2007) 2957–2961.
[4] N. Qin, M.M. Kržmanc, D. Suvorov, J. Am. Ceram. Soc. 91 (2008) 2593–2600.
[5] FIZ/NIST Inorganic Crystal Structure Database Version 1.2.1., Faschinformations zentrum, National Institute of Standards and Technology, Karlsruhe, Germany.
[6] Bruker Advanced X-ray Solutions TOPAS V2.0, User Manual. Bruker AXS, Version 2, Karlsruhe, Germany, 2000.
[7] A. March, Zeitschrift fur Kristallographie 81 (1932) 285–298.
[8] M. Jarvinen, J. Appl. Cryst. 26 (1993) 525–531.
[9] J.V. Smith, F. Rinaldi, Miner. Mag. 33 (1962) 202–211.
[10] R.D. Shannon, Acta Crystallogr. A 32 (1976) 751.
[11] J.V. Smith, W.L. Brown, Feldspar Minerals, second ed., vol. 1, Springer, 1988, pp. 63–66.
[12] J.V. Smith, Acta Crystllogr. 6 (1953) 613–620.
[13] R.D. Shannon, J. Appl. Phys. 73 (1993) 348–366.